www.sciencemag.org/cgi/content/full/1134548/DC1

Supporting Online Material for

Direct Measurements of the Convective Recycling of the Upper Troposphere

Timothy H. Bertram, Anne E. Perring, Paul J. Wooldridge, John D. Crounse, Alan J. Kwan, Paul O. Wennberg, Eric Scheuer, Jack Dibb, Melody Avery, Glen Sachse, Stephanie A. Vay, James H. Crawford, Cameron S. McNaughton, Antony Clarke, Kenneth E. Pickering, Henry Fuelberg, Greg Huey, Donald R. Blake, Hanwant B. Singh, Samuel R. Hall, Richard E. Shetter, Alan Fried, Brian G. Heikes, Ronald C. Cohen*

*To whom correspondence should be addressed. E-mail: cohen@cchem.berkeley.edu

Published 4 January 2007 on *Science* Express
DOI: 10.1126/science.1134548

This PDF file includes:

Supporting Online Material

1. INTEX-NA Experiment Description and Instrument Descriptions

The Intercontinental Chemical Transport Experiment – North America (INTEX-NA) took place between 1 July and 14 August 2004. Research flights were conducted out of Dryden Flight Research Center (Edwards AFB, CA), Mid-America Airfield (Mascoutah, IL); and PEASE International Trade-Port (Portsmouth, NH). Figure S1 depicts the vertical and horizontal extent of research flights conducted aboard the NASA DC-8 during INTEX-NA (*1*). DC-8 flight tracks are shown in the left panel of Figure S1 and the number of samples (10 second averaging time) in 1km vertical bins are shown in the right panel. *In situ* observations relevant to this study include; NO_2, HNO_3, OH, O_3, CO, CO_2, SO_2 and Ultra-fine Condensation Nuclei (UCN). Table S1 describes the detection threshold, uncertainty and time response for each measurement used in this analysis.

NO_2 LIF Instrument The NO_2 instrument flown aboard the DC-8 was described in detail by Thornton et al. (*2*), with specifics of the jet-expansion described by Cleary et al. (*3*). Briefly, NO_2 fluorescence is detected at 1Hz following excitation of a specific jet-cooled rovibronic transition in NO_2 at 585 nm. Red-shifted fluorescence is imaged at 90º onto an air cooled photomultiplier tube that is both optically and temporally filtered to remove laser scatter. NO_2 mixing ratios are calculated directly from fluorescence counts following calibration to NO_2 gas standards and measurement of the instrument zero from compressed air mixtures containing zero NO_2. Selectivity to NO_2 is demonstrated by tuning on and off of a specific NO_2 resonance, where the difference in observed fluorescence at the two different frequencies is attributed solely to NO_2. We calculate a

NO_2 detection threshold of 8 pmol mol^{-1} in 10 seconds at the surface and 25 pmol mol^{-1} in 10 seconds at the aircraft ceiling (12.5 km).

2. 0-D Time Dependent Model

The chemical evolution of convective outflow was modeled using a 0-D time dependent model. The model was initialized with chemical conditions, altitudes and detrainment times consistent with observations of fresh convection made during INTEX-NA. As time propagates in the model, we calculate the production and loss of O_3, CO, NO, NO_2, NO_3, N_2O_5, PAN, HO_2NO_2, HNO_3, OH, HO_2, RO_2, H_2O_2, CH_3OOH, H_2CO and C1-C6 hydrocarbons for 20 days following cloud detrainment. The conversion of NO_x to HNO_3 in the outflow region is used as an indicator of time since convection. Figure S2 depicts the results of a single run initialized at 10 km with a noon detrainment time. Initial conditions correspond to $[NO_x]_i$ = 800 pmol mol^{-1}, $[O_3]_i$ = 65 nmol mol^{-1} and $[CO]_i$ = 105 nmol mol^{-1}. Rapid conversion of NO_x to HNO_3 is observed during the first few days as the system approaches steady-state. In this analysis we assume: i.) HNO_3 is scavenged with unit efficiency in deep convection, ii.) γ_{N2O5} = 0.01 and iii.) HNO_3 is not scavenged by aerosols (or rain) following injection into the UT. All kinetic rates used in this analysis were taken from the NASA JPL Chemical Kinetics and Photochemical Data for Use in Atmospheric Studies, Evaluation Number 14 (*4*).

2.1 Treatment of OH and HO_2

The calculated time since convective detrainment is directly coupled to the HO_x budget through the daytime NO_x sink to HNO_3 via reaction with OH. As in other model

descriptions of the UT during INTEX-NA (*5*, *6*), our unconstrained model over-estimates OH by nearly a factor of two in the UT and under-estimates HO_2 by a similar amount. Due to the direct dependence of our timing indicator on HO_x, we constrain the mixing ratios of OH and HO_2 to the observed values as a function of NO_x and altitude. Figure S3 depicts the modeled mixing ratios of OH and HO_2 (lines), constrained to the observations (dots), as a function of NO_x and SZA at 10 km. The observed OH is a strong function of NO_x, while observations of HO_2 remain insensitive to NO_x. Constraints for OH and HO_2 were derived independently for each 1 km altitude bin. Constraining OH and HO_2 to the observations increases the time required for the NO_x-HNO_3 system to reach steady-state (by slowing the rate of OH + NO_2) and enhances the modeled O_3 production in the outflow region (by speeding up the rate of HO_2+NO).

2.2 Calculation of Time since Convection

The time since a sampled air-mass had been cloud processed is calculated by applying the mapping of time to NO_x/ HNO_3 (derived in the box model) to the observed NO_x to HNO_3 ratio. Figure S4 depicts the best-fit relation between the modeled NO_x to HNO_3 ratio and time since cloud processing at 10 km. This function is calculated at 1km increments from 6-12 km and applied to the measured NO_x to HNO_3 ratio.

2.3 Model Assumptions and Uncertainty

In order to access the uncertainty in the calculated time, we ran the time-dependent model under various different conditions encountered during INTEX-NA (e.g. $[NO_x]_i$ (0.2-3.0 nmol mol^{-1}), $[O_3]_i$ (40-100 nmol mol^{-1}), $[CO]_i$ (80-150 nmol mol^{-1}), detrainment time

(noon, 4PM local time, midnight), altitude (6-12 km) and time of year (June-September). As illustrated in Figure S4, the NO_x to HNO_3 ratio has good resolution (i.e. large rate of change per unit time) during the first five days following convection. Beyond five days small changes in NO_x/HNO_3 correspond to larger changes in the derived time. From the variance in the calculated time of individual model runs, we estimate the uncertainty in our modeled time to be ±6 hours at 1 day, ±12 hours at 2 days and ±1 day at 4 days. In addition, the INTEX-NA sampling domain did not permit frequent measurement of aged convection (>5 days). For these reasons we limit our analysis to the first five days following convection.

2.4 Treatment of Mixing

The mixing rate was determined by iterating the model until we had closure between the observed and modeled time evolution of a suite of long-lived species (e.g. CO, CH_4, CH_3OH and others). The modeled time rate of change of species X is determined as:

$$\frac{d[X]}{dt} = P(X) - L(X) - k_{dilution}\left([X] - [X]_{Background}\right)$$

where P(X) represents the chemical production of species X, L(X) represents the chemical loss of species X and $k_{dilution}$ is the mixing rate of the convective plume with background UT. We find this mixing term to be on average 0.05 ± 0.02 day^{-1}. That is, after 5 days, the plume still has 75% of its original contents. While individual convective plumes may mix faster (or slower) than this, the aggregate mixing rate of all the sampled plumes can be described by this rate. This rate supports the conclusion that over the course of 5 days, the convective plume remains relatively isolated from the background

UT. Background mixing ratios used in the dilution calculation were taken as the mean observed UT mixing ratios outside of fresh convective plumes.

Due to subsidence of convectively lofted air parcels following injection, our calculated time represents a lower bound for age as the chemical clock speeds up (due to NO_x repartitioning) as the parcel descends in altitude. However, this is a relatively small effect as calculated subsidence rates are approximately 35 hPa day^{-1} (*7*).

3.0 Comparison of Chemical and Meteorological Convective Influence Calculations

The results presented here provide a chemical constraint on the rate at which the UT over the continental US is influenced by convection during summer. In addition to the meteorological analysis of Fuelberg et al., presented in this manuscript, Thompson et al. assessed the effects of convection on the O_3 budget in the UT, over eastern North America, during the summer of 2004. Using results from the INTEX Ozone Sonde Network Study (IONS), the authors conclude that 10-15% (lower-limit) of the below tropopause O_3 can be attributed to the interaction of regional pollution with convection and lightning (*8*).

The INTEX-NA sampling period (June-August) and region (Eastern North America) is characterized by intense lightning activity. Cooper et al. calculated that 13% of the global annual lightning NO_x emissions occurred between 0º - 60º N and 135º - 60º W between June 21 and August 15, 2004 (*9*). In terms of lightning flash counts, Hudman et al., conclude that 2004 was typical (within 20% of the mean) of the past 5 years (*6*).

Persistent frontal passages prevented the formation of stagnant high pressure systems, typically observed during the summer over the northeastern United States (*10*). These frequent passages led to both record low temperatures and number of O_3 exceedances in the northeast (*11*). In contrast UT/LS O_3, as observed from the IONS network, was comparable to the climatology (*11*).

4.0 Measurement Uncertainties

In this analysis we calculate NO_x from observations of NO_2, O_3, HO_2 and photolysis rates measured directly on the DC-8. NO was measured directly on the DC-8 via a commercial grade chemiluminescence detector. The sensitivity of the chemiluminescence instrument (detection threshold > 50 pmol mol^{-1}) and long integration time (1 minute) prohibited its use in these calculations. NO was calculated from steady-state using the following equation:

$$[NO]_{Steady-State} = \frac{J_{NO_2}[NO_2]}{k_{NO+O_3}[O_3] + k_{NO+HO_2}[HO_2]}$$

We calculate the accuracy of the derived NO to be better than ± 30% based on the propagation of the individual errors used on the calculation. We calculate the precision of the derived NO to be better than ± 15% for typical values of NO_2, O_3 and JNO_2 found in the UT. Observations of nitrogen dioxide, ozone and JNO_2 made during the INTEX-NA campaign were compared directly with measurements made aboard the NOAA WP-3D during a series of in-flight comparisons. During these experiments the principal individual components used to derive NO_x (NO_2, O_3 and JNO_2) showed agreement to within their stated instrumental uncertainty.

In Figure S6 we compare the measured NO_x (using the chemiluminescence and the Laser Induced Fluorescence measurements) and NO_x calculated from steady-state for the entire INTEX-NA campaign. The steady-state NO_x agrees with the measured NO_x to within the calculated uncertainty when averaged to 1-minute and divided into 1km vertical bins. The observed upper tropospheric NO_x concentrations during INTEX-NA are on average much higher than previously reported on intensive aircraft field campaigns over North America. During the SUCCESS campaign, Jaeglé et al. report mean NO concentrations of 0.030 ± 0.022 nmol mol^{-1} and 0.061 ± 0.045 nmol mol^{-1}, for the altitude ranges of 8-10 km and 10-12 km, respectively (*12*). Crawford et al., report mean NO concentrations of 0.1 nmol mol^{-1} for observations made between 6-12 km during the SONEX campaign during the fall of 1997 over the North Eastern United States and the North Atlantic (*13*). Neither of these studies provides a direct comparison to the INTEX-NA data-set as SUCCESS was conducted in the spring and SONEX in the fall, while peak lightning and convection occurs over the continental North America during summer. The best comparison comes from NO_x measured aboard a commercial passenger aircraft during the NOXAR program between 1995 and 1997. Brunner et al. report a mean UT NO_x concentration of 0.4 nmol mol^{-1} during June, July and August over North America (*14*). As seen in Figure S6, our observations during the summer of 2004 are consistent with this.

We use the Caltech CIMS HNO_3 due to its fast time response (5 seconds as compared to 105 seconds for the UNH Mist Chamber Technique) and the UNH MC results when the

fast HNO_3 was unavailable. To account for the systematic bias between the two observations in the UT ($[HNO_3]_{UNH} = 0.6 \times [HNO_3]_{Caltech}$), we scale both the CIMS and MC observations to split the difference between the two measurements (i.e. we increase $[HNO_3]_{UNH}$ by 20% and decrease $[HNO_3]_{CIT}$ by 20%).

Due to the observed systematic bias, the choice of which HNO_3 measurement to use in the analysis has the potential to complicate our conclusions. To address these effects we have conducted the analysis using nitric acid as measured from: i.) the Mist Chamber – Ion Chromatography Instrument, ii.) the Chemical Ionization Mass Spectrometer and iii.) the scaled difference between the two techniques. The results are compared in Figures S7 and S8. Figure S7 shows the normalized frequency distribution in the time since convective influence, as calculated from observations of the NO_x to HNO_3 ratio made during the summer of 2004. Figure S8 depicts the fraction of air that had been influenced by convection within the past two days ($f_{< 2\ days}$) as a function of altitude. Calculations derived from the Mist Chamber – Ion Chromatography Instrument result in a higher fraction of convectively influenced air when compared with calculations made using measurements from the CIMS instrument. When compared with the results shown in Figure 6B of the manuscript, on which our conclusions regarding the convective overturn rate are drawn from, calculations using either the CIMS, MC-IC or the scaled difference result in a convective overturn rate between 0.1 and 0.2 day^{-1}.

2. Supplemental Figures

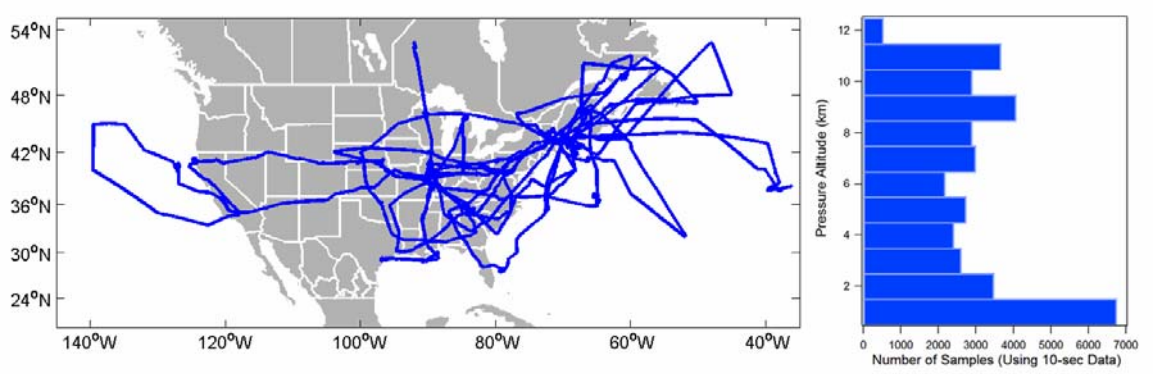

Figure S1: *left panel* INTEX-NA flight tracks made between 1 July 2004 and 14 August 2004 aboard the NASA DC-8. *right panel* Number of samples (using 10-sec averaged data) within 1km altitude bins between 0-12 km during the entire campaign.

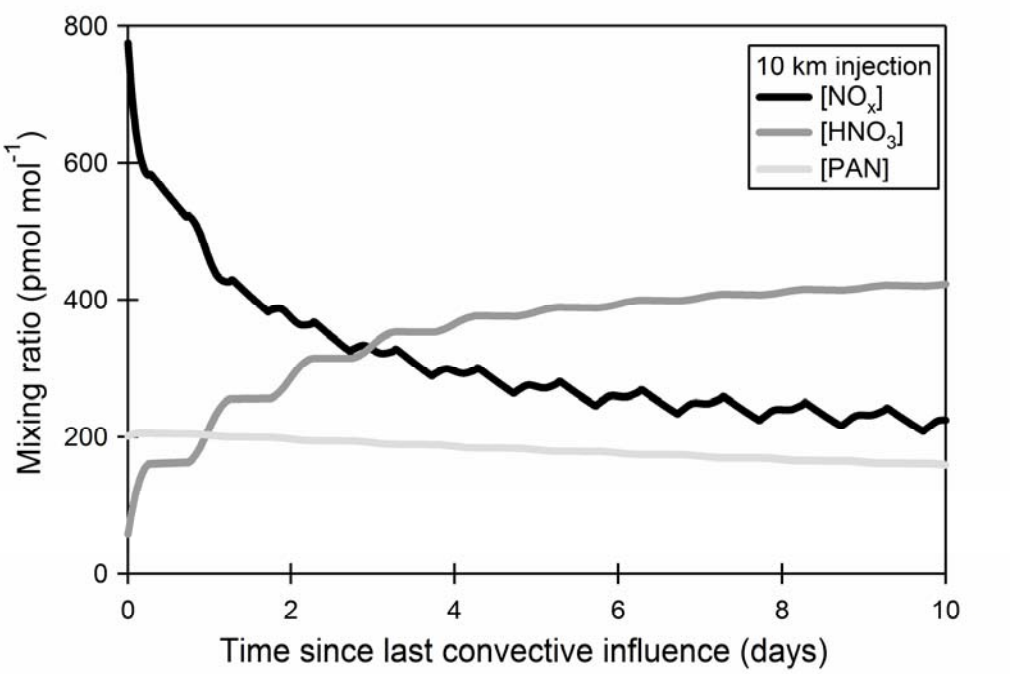

Figure S2: Time-dependent model illustrating the conversion of NO_x to nitric acid in the days subsequent to a cloud processing event occurring at 10 km. The above model was initialized at noon at 30º N in August using $[NO_x]_i$ = 800 pmol mol^{-1}, $[CO]_i$ = 105 nmol mol^{-1} at $[O_3]_i$ = 65 nmol mol^{-1}.

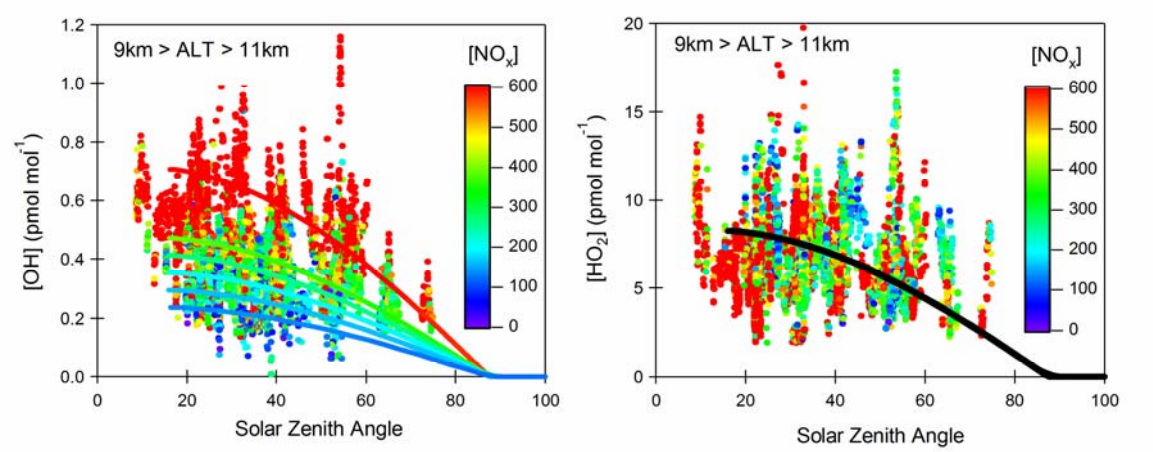

Figure S3: Model representation of OH (left panel) and HO_2 (right panel) as a function of SZA and $[NO_x]$. Model results (solid lines) are shown on top of the *in situ* observations (dots). The model was initialized at noon at 10km with $[NO_x]_i$ = 800 pmol mol^{-1}, $[CO]_i$ = 105 nmol mol^{-1} at $[O_3]_i$ = 65 nmol mol^{-1}. Observations shown were taken aboard the DC-8 between 9 and 11 km.

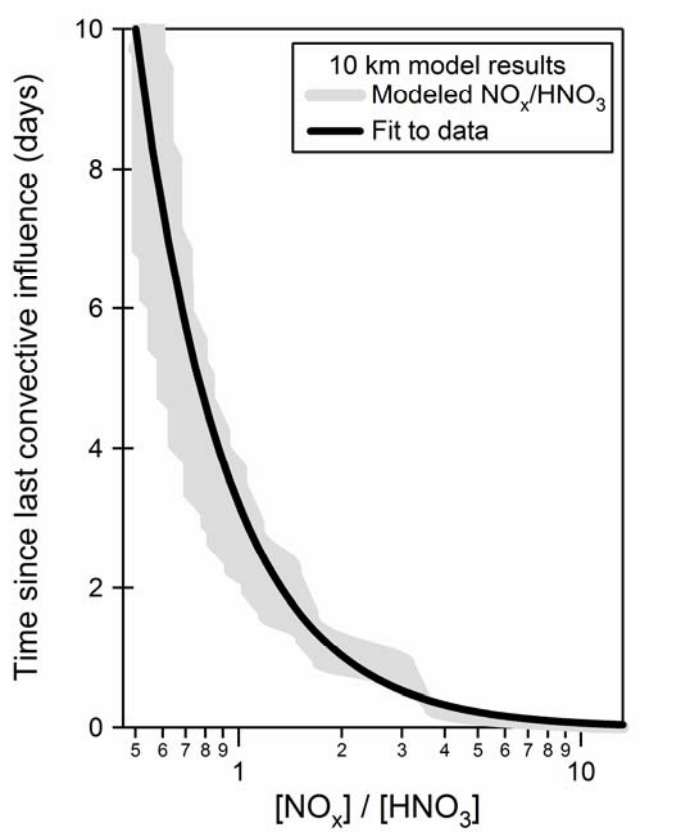

Figure S4: Observed NO_x to HNO_3 ratios are converted to a time since last convective influence using the best fit equation relating the NO_x/HNO_3 ratio to time as calculated using the time-dependent model in 1 km altitude bins from 7.5-11.5 km. The above equation is valid for pressure altitudes between 9.5 and 10.5 km.

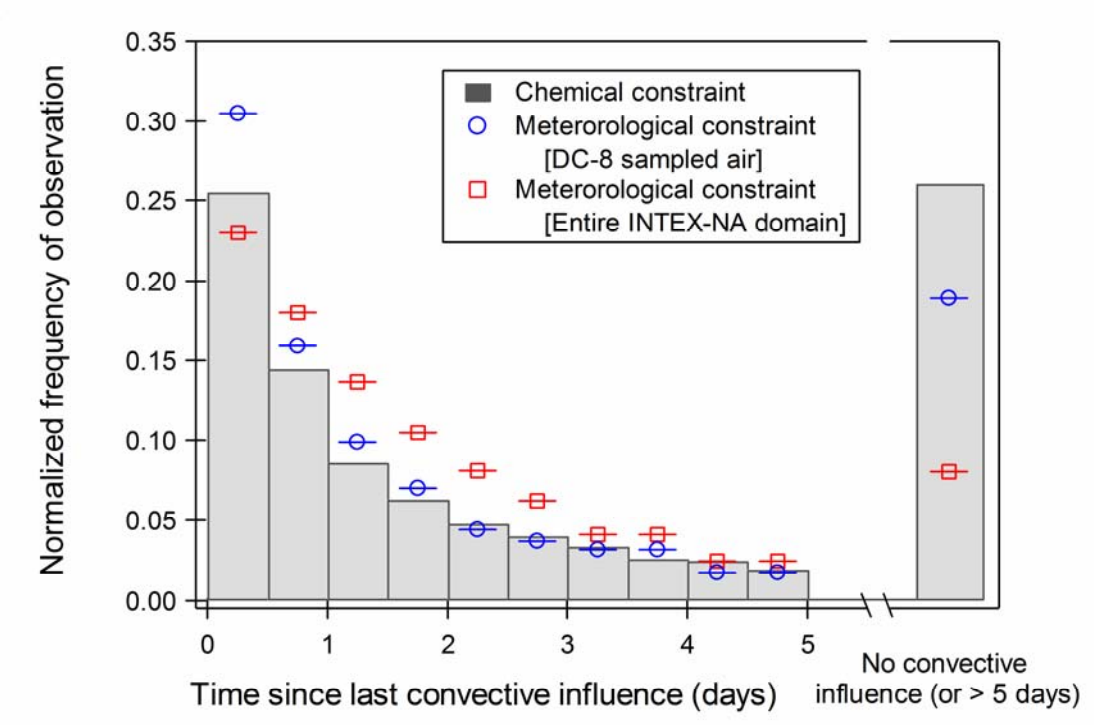

Figure S5: Comparison of chemical (grey bars) and meteorological constraints (-○-, -□-) on convective influence during INTEX-NA. Convective influence on air *sampled* by the DC-8 is shown with blue circles (-○-), while convective influence on the entire INTEX-NA domain is shown with red squares (-□-).

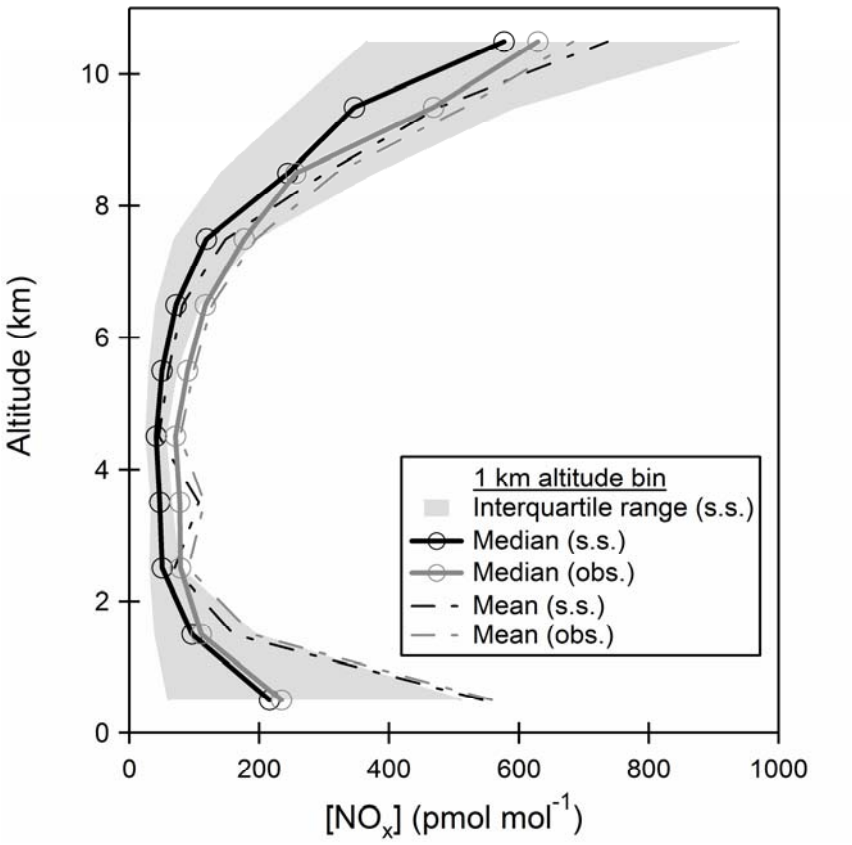

Figure S6: Comparison of observed (grey lines) and steady-state (black lines) NO_x for the entire INTEX-NA field campaign. The shaded region represents the interquartile range of the calculated NO_x.

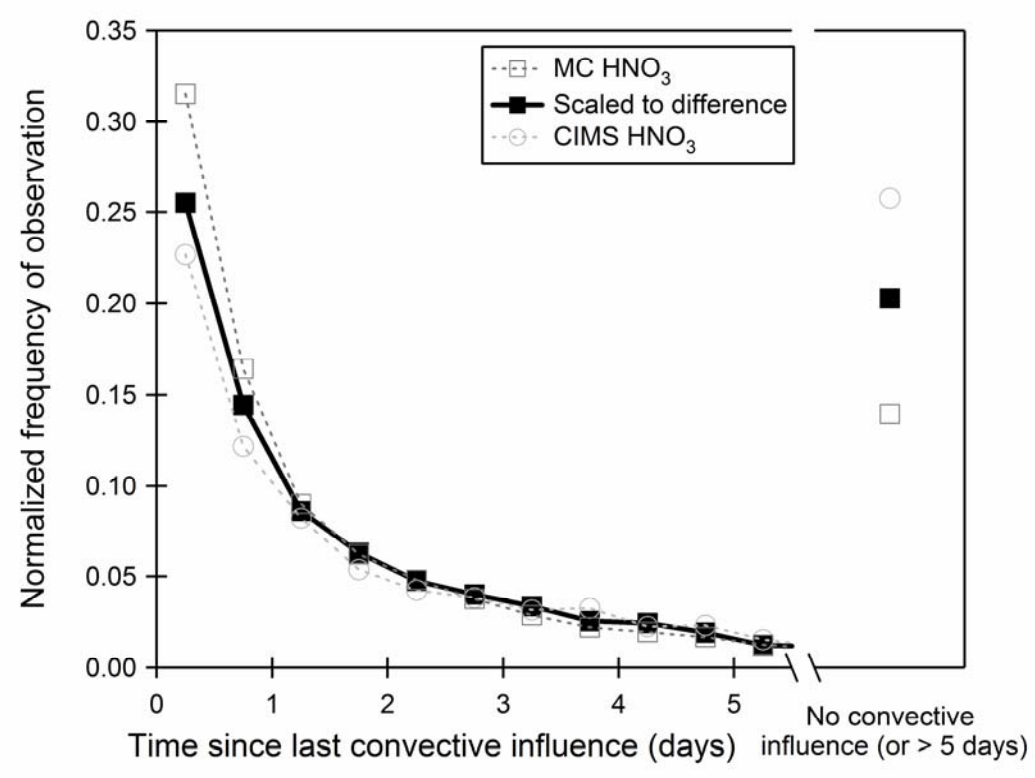

Figure S7: Normalized frequency distribution in the time since convective influence, as calculated from observations of the NO_x to HNO_3 ratio made during the summer of 2004. Calculations were conducted using nitric acid as measured from: i.) the Mist Chamber – Ion Chromatography Instrument (-□-), ii.) the Chemical Ionization Mass Spectrometer (-○-) and iii.) the scaled difference (-■-).

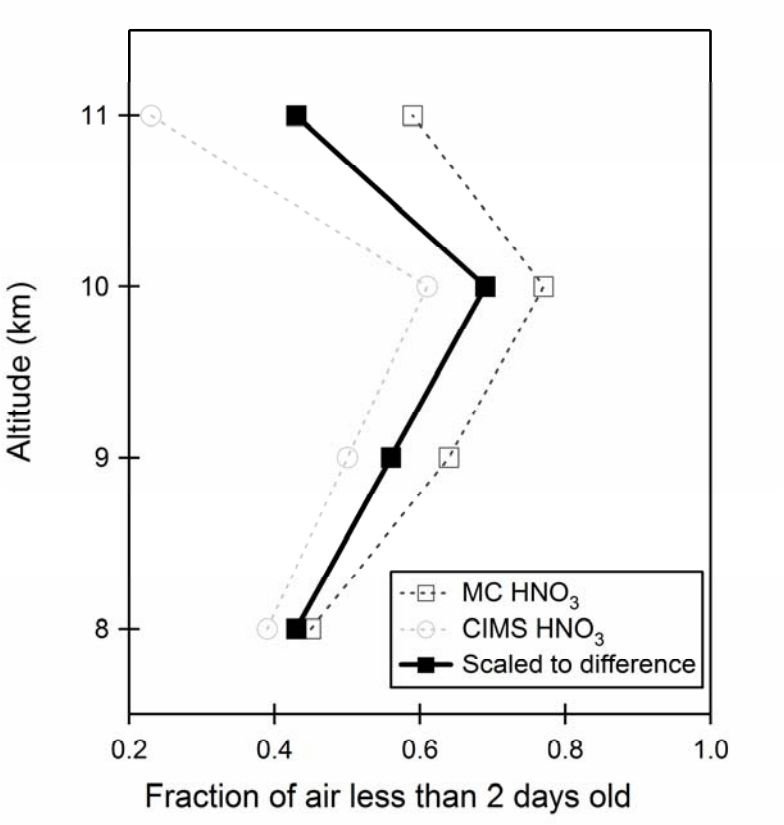

Figure S8: Fraction of air that had been influenced by convection within the past two days ($f_{< 2\ days}$) as a function of altitude. Calculations were conducted using nitric acid as measured from: i.) the Mist Chamber – Ion Chromatography Instrument (-□-), ii.) the Chemical Ionization Mass Spectrometer (-○-) and iii.) the scaled difference (-■-).

Species	Measurement Technique	Detection Threshold	Accuracy	Time Response	Reference
NO_2	LIF[1]	8 pptv / 10 sec See note 2	± 10% 1σ	1 Hz	(*2, 3*)
HNO_3	CIMS[3]	10 pptv / 0.5s	± 30%	0.5s sample every 5s	(*15*)
	Mist Chamber – IC[4]	5 pptv / 105 sec		105 sec	(*16*)
OH	LIF[1]	0.01 pptv	± 32% 2σ - 1 min	20 sec	(*17*)
O_3	Chemiluminescence	Precision = ±0.8ppbv, ±1% of reading	± 2 ppbv, ±3%	1 Hz	(*18*)
CO	IR-Absorption[5]	Precision = ±1ppbv, ±1% of reading (1σ)	± 3 ppbv, ± 3% 2σ	1 Hz	(*19*)
CO_2	IR-Absorption	Precision < 0.07 ppmv	± 0.25 ppmv	1 Hz	(*20*)
UCN, CN	TSI CPC[6]	See note 7	± 10%	1 Hz	(*21-23*)
J_{NO2}	Actnic Flux Spectroradiometer	4.1×10^{-7} sec^{-1}	± 11.9%	1 Hz	(*24, 25*)

[1]LIF – Laser Induced Fluorescence
[2]NO_2 detection threshold is 8 pptv / 10 sec at 760 Torr (ground) and 25 pptv / 10 sec at 200 Torr (10 km)
[3]CIMS – Chemical Ionization Mass Spectrometry
[4]IC – Ion Chromatography
[5]The accuracy and precision for CO were determined specifically for INTEX-NA (personal communication Glen Sachse)
[6]UCN (Ultra-fine Condensation Nuclei) was obtained by the difference of the UCN (D_p>3 nm, TSI 3025) and CN (D_P>10 nm, TSI 3010) Condensation Particle Counter (CPC) instruments.
[7]The TSI 3025 was a particle collection efficiency of 50% at 3 nm and 90% at 5 nm. The TSI 3010 has a particle collection efficiency of 50% at 10 nm.

Table S1: Detection thresholds, measurement uncertainty and time response of the *in situ* measurements used in this study. (Note: ppmv = μmol mol^{-1}, ppbv = nmol mol^{-1} and pptv = pmol mol^{-1})

References and Notes:

1. H. B. Singh, W. H. Brune, J. H. Crawford, D. J. Jacob, *Submitted J. Geophys. Res.* (2006).
2. J. A. Thornton, P. J. Wooldridge, R. C. Cohen, *Anal. Chem.* **72**, 528 (2000).
3. P. A. Cleary, P. J. Wooldridge, R. C. Cohen, *Appl. Optics* **41**, 6950 (2002).
4. S. P. Sander *et al.*, "Chemical Kinetics and Photochemical Data for Use in Atmospheric Studies, Evaluation Number 14" (National Aeronautics and Space Administration, Jet Propulsion Laboratory, California Institute of Technology, Pasadena, CA 2003).
5. X. R. Ren *et al.*, *Submitted J. Geophys. Res.* (2006).
6. R. C. Hudman *et al.*, *Submitted J. Geophys. Res.* (2006).
7. E. P. Salathe, D. L. Hartmann, *J. Climate* **10**, 2533 (1997).
8. A. M. Thompson *et al.*, *Submitted J. Geophys. Res.* (2006).
9. O. R. Cooper *et al.*, *In Press J. Geophys. Res.* (2006).
10. H. E. Fuelberg, M. J. Porter, C. M. Kiley, D. Morse, *Submitted J. Geophys. Res.* (2006).
11. A. M. Thompson *et al.*, *Submitted J. Geophys. Res.* (2006).
12. L. Jaegle *et al.*, *Geophys. Res. Let.* **25**, 1705 (1998).
13. J. Crawford *et al.*, *J. Geophys. Res.* **105**, 19795 (2000).
14. D. Brunner, J. Staehelin, D. Jeker, H. Wernli, U. Schumann, *J. Geophys. Res.* **106**, 27673 (2001).
15. J. D. Crounse, K. A. McKinney, A. J. Kwan, P. O. Wennberg, *Anal. Chem.* **78**, 6726 (2006).
16. R. W. Talbot *et al.*, *J. Geophys. Res.* **102**, 28303 (1997).
17. I. C. Faloona *et al.*, *J. Atmos. Chem.* **47**, 139 (2004).
18. M. A. Avery, *Submitted J. Oceanic and Atmos. Technol.* (2006).
19. G. W. Sachse, G. F. Hill, L. O. Wade, M. G. Perry, *J. Geophys. Res.* **92**, 2071 (1987).
20. B. E. Anderson *et al.*, *J. Geophys. Res.* **101**, 1985 (1996).
21. A. D. Clarke *et al.*, *J. Geophys. Res.* **109** (2004).
22. TSI Model 3010 Condensation Particle Counter Instruction Manual, TSI Inc. St. Paul, MN
23. TSI Model 3025 Condensation Particle Counter Instruction Manual, TSI Inc. St. Paul, MN
24. R. E. Shetter, M. Muller, *J. Geophys. Res.* **104**, 5647 (1999).
25. R. E. Shetter *et al.*, *J. Geophys. Res.* **108** (2003).